Solar Energy Materials & Solar Cells 225 (2021) 111020

Contents lists available at ScienceDirect

Solar Energy Materials and Solar Cells

journal homepage: http://www.elsevier.com/locate/solmat

Temperature-dependent performance of silicon solar cells with polysilicon passivating contacts

Anh Huy Tuan Le [a,*], Rabin Basnet [b], Di Yan [b], Wenhao Chen [b], Naomi Nandakumar [c], Shubham Duttagupta [c], Johannes P. Seif [a], Ziv Hameiri [a]

[a] School of Photovoltaic and Renewable Energy Engineering, University of New South Wales, Sydney, NSW, 2052, Australia
[b] Research School of Electrical, Energy and Materials Engineering, The Australian National University, Canberra, ACT, 2601, Australia
[c] Solar Energy Research Institute of Singapore (SERIS), National University of Singapore, Singapore, 117574, Singapore

ARTICLE INFO

Keywords:
TOPCon
MonoPoly™
POLO
Polysilicon
Passivating contacts
Temperature coefficient
Temperature dependence
Silicon solar cells

ABSTRACT

The temperature coefficient (TC) is a critical figure of merit to accurately evaluate the performance of solar cells at various operating temperatures, and hence, enabling the comparison between different cell technologies. Recently, tunnel oxide passivated contact (TOPCon) solar cells have shown outstanding cell performance. They are likely to be adopted in production lines and deployed in the field in the near future. Therefore, knowledge of their TCs and insights into their performance at realistic operating temperatures are of significant interest.

In this study, we investigate the temperature dependence of the performance of TOPCon solar cells and quantify their TCs. To gain better understanding regarding the temperature-dependent behavior of their performance, the passivation quality and the contact resistivity of polysilicon (poly-Si) passivating contacts as a function of temperature are investigated. Although an improvement of the passivation quality of these contacts with increasing temperature has been observed, it seems that this improvement weakly impacts on the open-circuit voltage TC. The cell performance at elevated temperatures is dominated by the drop in the open-circuit voltage, associated with the intrinsic carrier concentration related to band gap narrowing. The fill factor TC (TC_{FF}) is superior to those of other cell structures reported in the literature. We attribute this favorable TC_{FF} to the fact that some of the fill factor losses are compensated by the decrease of contact resistivity of the poly-Si passivating contacts at elevated temperatures. The relative TC of the cell efficiency of the investigated TOPCon cells is comparable to the TC of silicon heterojunction cells and it is superior to those of cell structures without passivating contacts. Moreover, we found that the investigated solar cell is more sensitive to temperature variation at lower illumination intensities.

1. Introduction

Photovoltaic (PV) devices are typically characterized at and optimized for standard testing conditions (STC; at 25 °C under an irradiance of 1000 W/m^2 and an AM1.5G solar spectrum) [1]. This, however, does not reflect the actual operating temperatures encountered in the field which significantly deviate from this standard [2]. It is well known that the operating temperature strongly effects the cell performance [2–4]. Therefore, knowledge regarding the temperature coefficients (TCs)—representing the temperature sensitivity of a solar cell [5]—is essential for cell optimization and for prediction of the power output from PV systems. Furthermore, TCs strongly depend on the cell structure [5]. The TC values vary between cell structures [2,3], which leads to a significant difference of their performance at relevant operating temperatures [2,3]. For an example, with almost identical efficiencies (≈21.6%) at STC, passivated emitter rear totally diffused (PERT) cells with a relative TC efficiency (TC_η) of −0.35 %/°C obtain an efficiency of 18.19% at 70 °C [3]. At the same operating temperature, silicon (Si) heterojunction (SHJ) cells with a relative TC_η of −0.29 %/°C present an efficiency of 18.70% [3], yielding a 0.51% absolute higher efficiency than that of the PERT cells. In general, the performance of Si-based solar cells is reduced at elevated temperatures [5]. It is well known that TC_η of these cells is dominated by the TC of the open-circuit voltage (TC_{Voc}) [5]. According to the literature, the higher the open-circuit voltage (V_{oc}), the lower the temperature sensitivity of the cells [5]. Therefore, cell structures enabling high V_{oc} values are expected to have a favorable TC_η.

* Corresponding author.
E-mail address: leanh619@gmail.com (A.H. Tuan Le).

https://doi.org/10.1016/j.solmat.2021.111020
Received 7 October 2020; Received in revised form 9 February 2021; Accepted 12 February 2021
Available online 23 March 2021

Recently, passivating-contact-based solar cells have been developed [6–11]. These structures simultaneously minimize recombination losses at the interfaces of the base, while effectively collecting only one type of charge carrier (electrons or holes) [7,12–15]. Solar cells based on this concept show a high potential to obtain excellent performance [16–21] with a record V_{oc} of up to 750 mV [22]. Among them, solar cells with polysilicon (poly-Si) passivating contacts not only exhibit outstanding cell performance, but may also be easily introduced into existing PV production lines [6,16,18,23–25]. These contacts are formed by an ultra-thin silicon oxide (SiO_x) film and a doped poly-Si layer. Haase *et al.* reported the current efficiency record of 26.1% for an interdigitated back-contacted solar cell using a SiO_x/poly-Si stack [16]. Furthermore, a 244.3 cm^2 bifacial monoPoly™ solar cell fabricated by an industrial inline plasma-enhanced chemical vapor deposition (PECVD) has been reported with an efficiency of 22.8% [18]. So far, the performance of these solar cells has been mainly measured under the STC. To our knowledge, there is no published report regarding their efficiency TC. Note that different terms are used to name solar cells with poly-Si passivating contacts such as TOPCon (tunnel oxide passivated contact) [25], POLO (poly-Si on oxide) [26], and monoPoly™ [27,28]. In this paper, these cells are mostly referred to as TOPCon solar cells.

In this study, we examine the performance of TOPCon solar cells with a front boron diffusion in the temperature range from 25 to 70 °C. The TCs of different cell parameters are determined and compared to values reported for other solar cell structures. The series resistance (R_s) and shunt resistance (R_{sh}) of the cells are extracted in the same temperature range and correlated to the trend of the fill factor (*FF*). We also investigate the contact resistivity (ρ_c) and the saturation current density (J_{0s}) of poly-Si passivating contacts as a function of temperature in order to gain a better understanding regarding their impact on TC_{FF} and TC_{Voc}, respectively.

2. Experimental details

2.1. Sample preparation

In this study, TOPCon solar cells were fabricated using compensated Czochralski-grown upgraded metallurgical-grade (UMG-Cz) n-type Si wafers with a resistivity of 1.2 Ω·cm and a thickness of 150 ± 10 μm. The wafers were saw damage etched prior to Radio Corporation of America (RCA) cleaning [29]. A *tabula rasa* treatment, that has been optimized for UMG-Cz Si wafers [30], is applied. The front surface of the wafers was textured using a wetting agent prior to forming the front hole-collector with a sheet resistance of 130–140 Ω/□ by a boron diffusion. Further details can be found in Ref. [23]. A poly-Si passivating contact was then defined at the rear. This was achieved by growing a 1.4-nm-thin SiO_x layer using a 68% nitric acid solution, followed by deposition of an intrinsic amorphous-Si film of 50 nm by PECVD. Phosphorus diffusion using a furnace at 820 °C for 25 min and a drive-in for 30 min was then performed to simultaneously dope and crystallize the amorphous-Si film, resulting in an n-type poly-Si layer. Further details of this diffusion process can be found in Ref. [31]. A stack layer of atomic layer deposited aluminum oxide and PECVD silicon nitride (SiN_x) films was used for front surface passivation and antireflection. The front metal grid was formed by evaporating a chromium/palladium/silver stack through a mask. An evaporated silver (Ag) layer of 600 nm is used as the full rear contact. A sketch of the finished device is shown in Fig. 1(a). Solar cells with an active area of 2 × 2 cm^2 were cut from larger wafers after processing. Photoluminescence images taken after cleaving indicate a good uniformity of all the cells.

To investigate the temperature dependence of the poly-Si passivating contacts, two different test structures are used. Symmetrical lifetime test structures as shown in Fig. 1(b) are used for effective lifetime (τ_{eff}) measurements and J_{0s} extraction. These structures were fabricated using high-resistivity n-type float-zone (FZ) Si wafers (310 ± 10 μm, 100 Ω·cm) with poly-Si passivating contacts on both sides. Such wafers allow

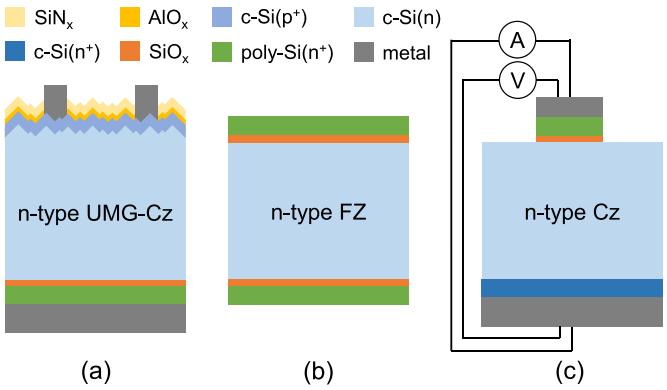

Fig. 1. Sketch of (a) the UMG-Cz TOPCon solar cells, (b) symmetrical test structures for effective lifetime measurements, and (c) a Cox and Strack test structure for extraction of the contact resistivities.

both uniform excess carrier concentration across the wafer's depth and measurements at high injection, satisfying the requirements of the Kane-Swanson method [32]; they are, therefore, commonly used for J_{0s} extraction [31,33,34]. ρ_c was determined using the Cox and Strack test structures [35], defined on n-type Cz Si wafers (290 ± 10 μm, 2 Ω·cm). Poly-Si passivating contacts were applied only to one side of these structures. Circular metal contacts with various diameters were formed on top of the poly-Si film by evaporating Ag through a shadow mask, while a full Ag metal contact was evaporated on the opposite ('rear') side, as shown in Fig. 1(c). The poly-Si layer around the circular pads was etched back to avoid spreading currents. Note that besides doping and crystallizing the amorphous-Si film, the phosphorus diffusion also creates a highly doped n-type layer at the rear side of these test structures. The oxide was removed from the rear side prior the diffusion.

To validate our results, state-of-the-art n-type Cz monoPoly™ busbar-less solar cells are used [18]. The monoPoly™'s structure also includes a front boron diffusion and a rear n-doped poly-Si passivating contact. These cells were fabricated on 6-inch wafers with a resistivity of 1.1 Ω·cm and a thickness of 160 ± 10 μm. Since our facilities do not support current-voltage (*I–V*) measurements of busbar-less cells, front busbars and a full rear metal contact were formed by evaporating 1-μm aluminum (Al) layers. Comparison between *I–V* measurements before (as provided by the partner) and after this additional metallization process indicates an identical V_{oc} and a minor reduction of the short-circuit current (J_{sc}) that can be fully explained by additional shading. However, as the grid of these cells is designed for a busbar-less structure, the obtained *FF* after the metallization process is lower than the *FF* measured by the partner. Therefore, only the TC_{Voc} and TC_{Jsc} of these cells are used for comparison.

2.2. Characterization

To investigate the temperature dependence of the cell parameters, *I–V* testers and a customized Suns-V_{oc} [36] system are used. *I–V* measurements are done from 25 to 70 °C, while Suns-V_{oc} measurements are performed cooling down the sample from 80 to 30 °C. Determination of R_s is done by comparing the one-sun current density-voltage (*J-V*)—series-resistance affected—curve to the series-resistance-free *J-V* curve obtained from the Suns-V_{oc} measurements using the following equation [37]:

$$R_s = \frac{\Delta V}{J_{mpp}} \quad (1)$$

where ΔV is the voltage difference between the *J-V* curves at the maximum power point of the one-sun *J-V* curve, and J_{mpp} is the current density at this point.

The cells' R_{sh} is determined from the slope (linear fit) of the one-sun

J-V curves around $V = 0$ V. To determine ρ_c of poly-Si passivating contacts, the *I–V* characteristics of the Cox and Strack test structures are measured in the dark, varying the temperature from 25 to 80 °C. Here we assume that the ohmic contact at the rear side of these structures has a negligible contribution to the total measured resistance (R_{total}). Hence, our measurements represent the upper limit of the extracted ρ_c. It should be noted that the extracted ρ_c represents a lumped value consisting of the contact resistivities of the Si/SiO_x, SiO_x/poly-Si, and poly-Si/Al interfaces, as well as the poly-Si bulk resistivity.

A customized lifetime tester [38] is used for τ_{eff} measurements in the temperature range from 25 to 80 °C. Extraction of J_{0s} is done using the curve fitting features of Quokka 2 [39] and the approach of Dumbrell *et al.* [40]. R-squared is used to evaluate the fit quality. The band gap narrowing model of Schenk [41] is used for the calculation of the effective intrinsic carrier concentration ($n_{i,eff}$) [42], whereas the models of Richter *et al.* [43] and Klaassen [44] are applied for the determinations of the intrinsic lifetime and the mobility, respectively.

The TCs are extracted from the slopes of linear fits of the cell parameters as a function of temperature. All the TCs are normalized to the value at 25 °C and reported as relative TC values in this study.

3. Results and discussion

3.1. Temperature dependence of TOPCon and monoPoly™ solar cells

The temperature dependence of electrical parameters of the UMG-Cz TOPCon and Cz monoPoly™ solar cells at one-sun is shown in Fig. 2(a)–(d). Photoluminescence images (see Fig. 1S in the supplementary information) indicate a good uniformity of both cells. Linear trends as a function of temperature are observed for all the parameters of both cells. As expected, J_{sc} increases at elevated temperatures while V_{oc}, *FF,* and the obtained efficiency decrease [5]. This decrease is related to the increase in $n_{i,eff}$ at elevated temperatures caused by the narrowing of the band gap energy (E_g) [45]. Similar trends for V_{oc} and *FF* have been previously reported for TOPCon solar cells by Feldmann *et al.* [46]. On the other hand, the reduction of E_g with increasing temperature explains the increase of J_{sc} [5]. The figure also presents the temperature dependence of the pseudo fill factor (*pFF*). It is noteworthy that the decrease of *pFF* with temperature—obtained from temperature-dependent Suns-V_{oc} measurements—is more pronounced than the reduction observed for the *FF*. This difference can be used to assess the contribution of R_s to the temperature dependence of *FF*, as will be discussed in Section 3.3. The extracted TCs are summarized in Table 1.

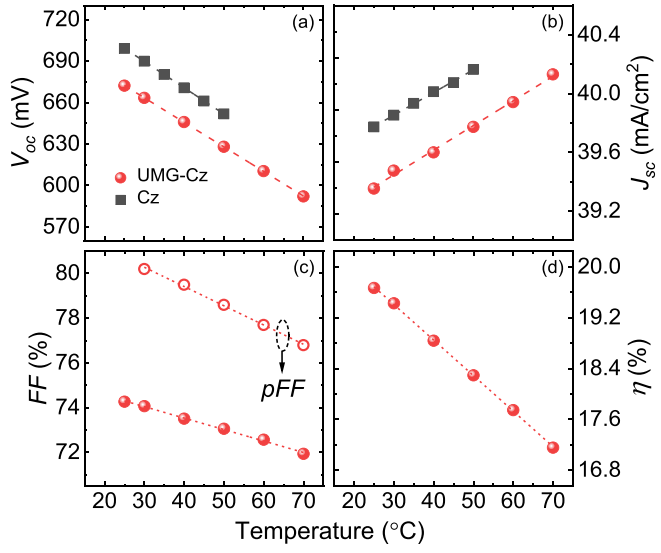

Fig. 2. Cell parameters of the UMG-Cz TOPCon and Cz monoPoly™ solar cells including (a) V_{oc}, (b) J_{sc}, (c) *FF* and *pFF* (open points), and (d) efficiency (η) under one-sun illumination as a function of temperature.

It is noteworthy that the TC_{Voc} values of the UMG-Cz TOPCon and Cz monoPoly™ solar cells are nearly equal, despite of the difference of their V_{oc} at STC. It is well known that the TC_{Voc} of well-performed Si-based solar cells depends on both the V_{oc} at STC and the constant factor gamma (γ)—introduced by Green [5]—as described in the following equation [47]:

$$TC_{V_{oc}} = \frac{dV_{oc}}{dT} \times \frac{100}{V_{oc(STC)}} = -\frac{E_{g0}/q - V_{oc} + \gamma k_B T/q}{T} \times \frac{100}{V_{oc(STC)}} \quad (2)$$

where E_{g0} is the semiconductor band gap linearly extrapolated to 0 K, q is the elementary charge, k_B is the Boltzmann constant, T is the temperature, and $V_{oc(STC)}$ is the V_{oc} of the cell at STC. γ includes the temperature dependence of parameters that determine the diode saturation current density, and hence, contains information about the dominant recombination mechanism in the cell [48,49]. Because the V_{oc} of the Cz monoPoly™ cell at STC (699.1 mV) is higher than that of the UMG-Cz TOPCon cell (672.2 mV), the similar TC_{Voc} of these cells might be due to different gamma factors. Assuming E_{g0} of 1.206 eV, the calculated γ of the Cz monoPoly™ and UMG-Cz TOPCon cells at STC based on Equation (2) are +2.31 and −0.16, respectively. γ is usually lying within the range from one to four [47–49]. However, negative γ values have been observed and discussed in the literature [50–53]. Dupré *et al.* attributed it to a substantial increase of external radiative efficiency (ERE) of the cell with increasing temperature at the open circuit condition [50]. This might be related to a weaker reduction of the minority carrier mobility in the UMG-Cz TOPCon cells using compensated wafers, as will be discussed below.

The TCs obtained in this study (of cells with front boron diffusion) are compared to TCs of other solar cell structures [3] and presented in Fig. 3(a)-(d), while the contributions of each TC to the obtained TC_η are depicted in Fig. 3(e).

The investigated cells' TC_{Voc} in this study seems to be superior to those of the cells without passivating contacts [aluminum back surface field (Al-BSF), passivated emitter and rear contact (PERC), PERT and advanced PERT cells]. It is slightly worse than the TC_{Voc} of the SHJ cells. Part of the difference can be explained by the lower V_{oc} values of 672 and 699 mV at STC (UMG-Cz TOPCon and Cz monoPoly™) compared to the 733 mV of the SHJ cell [3]. It is probably since the SHJ cells have passivating contacts on both sides. As expected, TC_{Voc} has the larger impact on TC_η, contributing more than 60% at any cell structure.

The TC_{Jsc} of the UMG-Cz TOPCon cells is higher than most of the other cell structures and is comparable to that of the Al-BSF cells. For Si-based solar cells, J_{sc} is strongly impacted by the minority carrier diffusion length that is determined by the product of τ_{eff} and the minority carrier mobility [54]. The latter is impacted by different scattering sources [55]. For Si wafers, lattice and ionized impurity scatterings are two of the main scattering effects that limit the mobility [54]. At elevated temperatures, the mobility that is limited by lattice scattering (μ_{lat}) is strongly reduced due to an increase of the interactions between carriers and phonons, whereas the mobility that is limited by ionized impurity scattering (μ_{imp}) is improved [56]. For low and moderately doped wafers, the former process is dominant. However, for compensated wafers in which the doping concentrations of both dopants are

Table 1
Extracted TCs and their statistical errors of the linear regression of the UMG-Cz TOPCon and Cz monoPoly™ cells.

	TC_{Voc} (%/°C)	TC_{Jsc} (%/°C)	TC_{FF} (%/°C)	TC_{pFF} (%/°C)	TC_η (%/°C)
UMG-Cz	−0.264 ± 0.001	+0.048 ± 0.002	−0.069 ± 0.001	−0.101 ± 0.002	−0.285 ± 0.005
Cz	−0.271 ± 0.001	+0.043 ± 0.002			

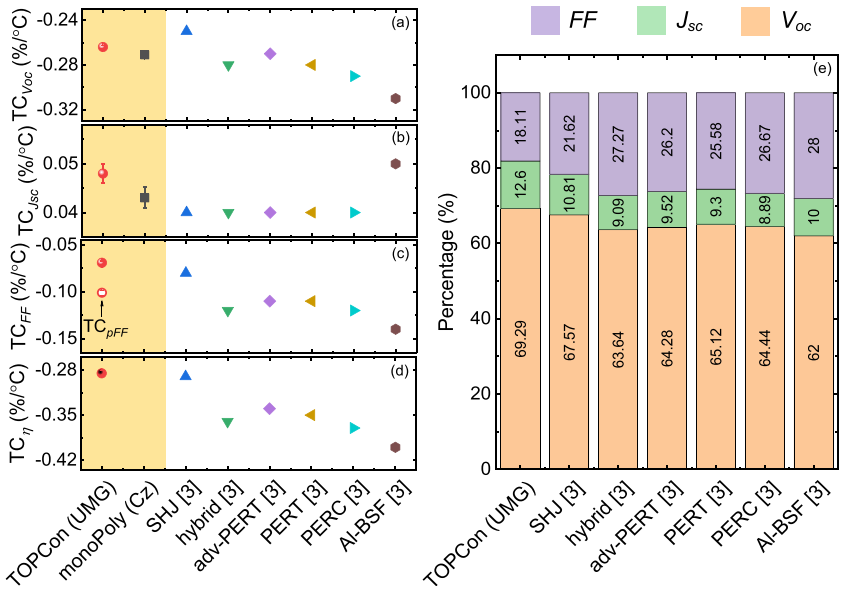

Fig. 3. (a) TC_{Voc}, (b) TC_{Jsc}, (c) TC_{FF} and TC_{pFF}, and (d) TC_{η} of the UMG-Cz TOPCon and Cz monoPoly™ solar cells extracted from the slopes of linear fits of the cell parameters as a function of temperature as shown in Fig. 2. Error bars are obtained from the linear fits. TCs of other solar cell structures reported in Ref. 3 are also shown for comparison. (e) Percentage contribution of TC_{Voc}, TC_{Jsc}, and TC_{FF} to TC_{η} of the UMG-Cz TOPCon solar cells and other cell structures.

high, ionized impurity scattering becomes significant [56]. Consequently, the improvement of μ_{imp} with increasing temperature is counterbalanced by the reduction of μ_{lat}, resulting in a weaker temperature dependence of the minority carrier mobility in compensated wafers. Therefore, we attribute the superior TC_{Jsc} of the UMG-Cz TOPCon cells using compensated wafers to a weaker reduction of the minority carrier mobility with increasing temperature [56,57]. A similar phenomenon is observed for PERT fabricated using compensated wafers [58]. The contribution of TC_{Jsc} to TC_{η} is the smallest for all the cell structures [see Fig. 3 (e)].

Note that the TC_{Jsc} of the Al-BSF cells is superior to those of other cell structures. It is well known that a well-designed rear dielectric passivation layer can suppress the parasitic absorption occurring at the rear metal contact [59,60]. The absence of such a layer in the Al-BSF cells could lead to significant parasitic absorption at the metal reflector. The light absorption of the bulk is increased with increasing temperature due to band gap narrowing [5]. Thus, less light reaches the rear, leading to a reduction of the parasitic absorption at the rear metal contact. Therefore, compared to the value at STC, the relative increase of the Al-BSF cells' J_{sc} at elevated temperatures is higher than that of other cell structures with a rear dielectric passivation or low refractive index layer.

The TC_{FF} of TOPCon cells of this study is superior to all TC_{FF}s reported in Ref. [3]. Furthermore, their contribution to TC_{η} is the smallest compared to other cell structures. As mentioned earlier [Fig. 2(c)], TC_{FF} is better than TC_{pFF} (by 0.032 %/°C). This is due to the reduction of R_s with increasing temperature and can be correlated to ρ_c of poly-Si passivating contacts and other components, as will be discussed in Section 3.3.

The TC_{η} of the investigated TOPCon solar cells (−0.285 %/°C) is comparable to that of SHJ (−0.29 %/°C) and better than the coefficients of solar cell structures without passivating contacts, highlighting the advantage of using these advanced structures in the field.

3.2. Injection and temperature dependence of TOPCon solar cells

In the previous section, we focused on cell parameters at one-sun. It is interesting to examine the temperature dependence of the cell performance across a larger range of illuminations. Suns-V_{oc} measurements in the temperature range from 30 to 80 °C are presented in Fig. 4(a). At low illumination intensities, the cell voltage shows a significant drop. The Suns-V_{oc} curve measured at 30 °C exhibits noticeable bending in this illumination intensity region. With increasing temperatures, the prominence of this voltage drop is reduced, and the bending disappears almost completely at 80 °C. At high illumination intensities, the increase of the cell voltage with increasing illumination intensities becomes less pronounced, which can be explained by a Schottky barrier at the rear side of the cells [61–63]. In this study, the poly-Si passivating contact is integrated into the rear. Therefore, a formation of a Schottky barrier can be assumed at the Si/SiO_x interface, as also discussed by Folchert *et al.* [64]. This will be discussed further in Section 3.3.

From the Suns-V_{oc} curves, we extract relative TC_{Voc} values (green circles) as a function of illumination intensity and present them in Fig. 4 (b). For comparison, TC_{Voc} values obtained from *I–V* measurements (red squares) are also shown. It is clearly seen that the TC_{Voc} values extracted from both measurement methods match well. For most of the range, the absolute value of determined TC_{Voc} decreases with increasing illumination intensity. The investigated solar cell is more sensitive to temperature variation at lower illumination intensities.

3.3. Temperature dependence of R_{sh} and R_s

In Section 3.1, it was shown that the TC_{FF} of the UMG-Cz TOPCon

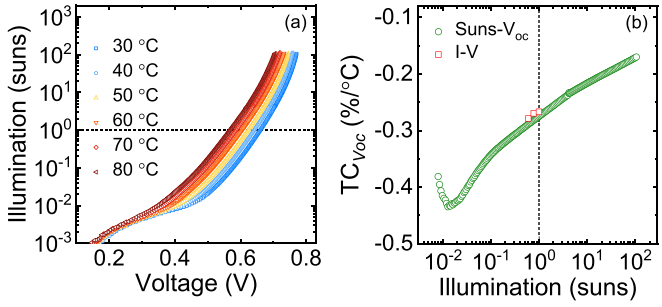

Fig. 4. (a) Suns-V_{oc} measurements of the UMG-Cz TOPCon solar cell at different temperatures and (b) TC_{Voc} extracted from Suns-V_{oc} (green circles) and *I–V* (red squares) measurements as a function of illumination intensity. (For interpretation of the references to colour in this figure legend, the reader is referred to the Web version of this article.)

cells is better than those of other cell structures. This section investigates several components that impact TC_{FF} to explain this finding.

The temperature dependence of both R_s and R_{sh} of the UMG-Cz TOPCon cells is presented in Fig. 5. It seems that both parameters decrease linearly with increasing temperature. The TCs of R_s (TC_{Rs}) and R_{sh} (TC_{Rsh}) are −0.812 %/°C and −1.231 %/°C, respectively. The reduction of R_{sh} of Si-based solar cells at elevated temperatures has been reported in the literature [65,66]. However, no detailed explanation for this reduction was presented in these references. Singh *et al.* reported a TC_{Rsh} of −0.700 %/°C for Al-BSF cells [65] while a value of −1.021 %/°C was measured by Cuce *et al.* for monocrystalline-Si-based cells [66]. Both values are superior to the measured TC_{Rsh} of the cells in this study. The physics behind the R_{sh} reduction at elevated temperatures is still unclear and requires further investigation.

The cell's R_s comprises the following components:

$$R_s = R_{m,r} + R_{m/poly} + R_{poly} + R_{poly/SiOx/bulk} + R_{bulk} + R_h + R_{h/m} + R_{m,f} \quad (3)$$

where $R_{m,r}$, R_{poly}, R_{bulk}, R_h, and $R_{m,f}$ are the contributions of the rear metal contact, the poly-Si layer, the Si wafer, the front hole-collector, and the front metal contacts including fingers and busbars, respectively. The contributions of the interfacial contacts, including the rear-metal/poly-Si, poly-Si/SiO_x/Si, and front hole-collector/metal interfaces, to R_s are named as $R_{m/poly}$, $R_{poly/SiOx/bulk}$, and $R_{h/m}$. Due to the reduction of carrier mobility with increasing temperature from 30 to 70 °C [44], R_{bulk} is increased. The cell's R_h is determined by the spacing between fingers and the sheet resistance of the front hole-collector [67]. Due to a high doping concentration in this collector (a sheet resistance of 130–140 Ω/□), the reduction of the carrier mobility is negligible at elevated temperatures [44], resulting in a minor increase of R_h. Therefore, the increases of R_{bulk} and R_h with temperature cannot explain the trend of R_s. We expect to correlate the drop in R_s at elevated temperatures with the temperature-dependent behavior of $R_{m/poly}$, R_{poly}, $R_{poly/SiOx/bulk}$, $R_{m,r}$, $R_{h/m}$, and $R_{m,f}$. The information regarding the first four components as a function of temperature can be obtained from the ρ_c test structure.

3.3.1. Temperature dependence of contact resistivity

The *I–V* characteristics of the Cox and Strack test structures with the front electrode diameter of 3 mm in the temperature range from 25 to 80 °C are depicted in Fig. 6(a). Ohmic contact behavior is observed for the entire investigated temperature range. When increasing the temperature, R_{total} is reduced, indicating a decrease of ρ_c of the poly-Si passivating contact. Similar ohmic behavior and R_{total} trend with temperature are observed for other measurements using front electrodes

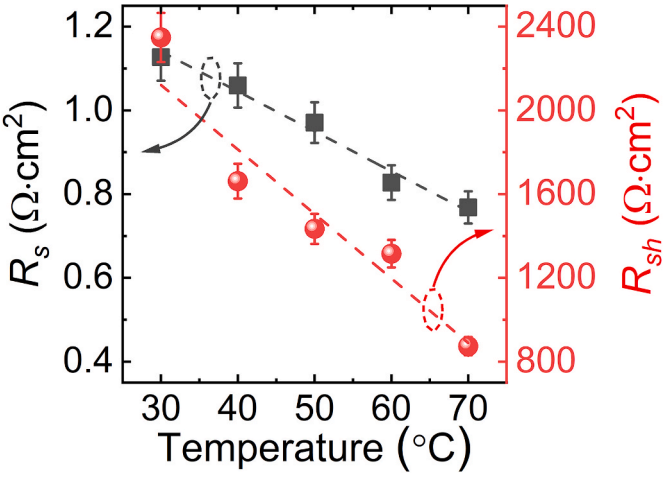

Fig. 5. R_s and R_{sh} of the UMG-Cz TOPCon solar cell as a function of temperature.

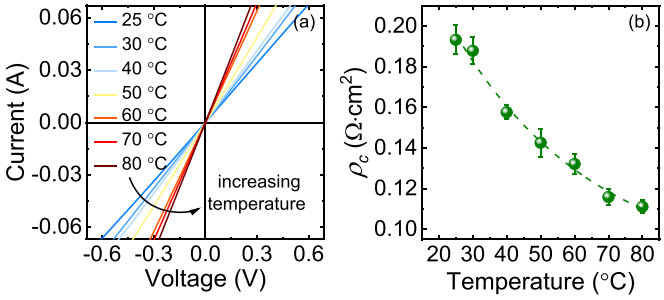

Fig. 6. (a) *I–V* characteristics of the ρ_c test structure with the front electrode diameter of 3 mm, and (b) ρ_c extracted using the Cox and Strack method as a function of temperature. The error bars are calculated from ρ_c fits. The dashed line is an exponential fit based on the model proposed by Folchert *et al.* [64].

with diameters from 0.5 to 10 mm. Extracted ρ_c values from *I–V* measurements as a function of temperature are shown in Fig. 6(b). When the temperature is increased from 25 to 80 °C, ρ_c decreases from 0.19 to 0.11 Ω·cm². As discussed previously, this improvement of ρ_c with temperature offsets the contributions of $R_{m/poly}$, R_{poly}, and $R_{poly/SiOx/bulk}$. It is noteworthy that the decrease of ρ_c is smaller than that of R_s in the same temperature range. Hence, the R_s reduction at elevated temperatures cannot be solely explained by the decrease of ρ_c. Nevertheless, it seems that the improvement of ρ_c at higher temperatures counterbalances some of the *FF* losses, and hence, improves TC_{FF}. The remaining contributions to the R_s reduction might be from $R_{m,r}$, $R_{h/m}$, and $R_{m,f}$. The quantification of these parameters is out of the scope of this study. Note that the metal contacts used in the Cox and Strack structures were formed by evaporating Ag and not by industrial approaches, such as screen printing or plating.

The temperature-dependent ρ_c of poly-Si passivating contacts was also investigated by Folchert *et al.* [64]. They used two extreme cases of (a) tunnelling-dominant transport and (b) pinhole-dominant transport samples to extract ρ_c as a function of temperature. They observed that ρ_c decreases at elevated temperatures for the former and *vice versa* for the latter. For the case of tunneling-dominated transport samples, the carrier transport was modeled based on a Schottky barrier at the Si/SiO_x interface [64]. For the pinhole-dominant transport samples, the semi-classical drift-diffusion model was used to describe the transport through pinholes [64]. As a reduction of ρ_c with increasing temperature is observed in our study, we assume that the carrier transportation in our samples is dominated by tunneling. Moreover, as mentioned in Section 3.2, the behavior of the cell voltage with increasing illumination intensity indicates a Schottky barrier at the rear side of the TOPCon solar cells. This Schottky barrier can be attributed to the barrier at the Si/SiO_x interface. This supports our assumption that tunneling transport is dominating the carrier transport at the studied poly-Si/Si interface. Note that $R_{m/poly}$ which is derived from the barrier at the metal/poly-Si interface might have a similar temperature-dependent behavior as ρ_c. Since the quantification of each component of ρ_c is out of the scope of this study, the possibility that $R_{m/poly}$ dominates the temperature-dependent behavior of ρ_c might not be excluded.

3.4. Temperature dependence of poly-Si passivation

From the symmetrical lifetime test structures, τ_{eff} as a function of the excess carrier concentration (Δn) at different temperatures is extracted and presented in Fig. 7(a). An increase of τ_{eff} over the entire measured injection level range is observed. This improvement is less pronounced at high injection levels due to the dominance of Auger recombination in this injection range. Using Quokka 2, J_{0s} is extracted from the τ_{eff} measurements and presented in Fig. 7(b). A significant increase of J_{0s} with temperature is observed. As $n_{i,eff}$ increases by several orders of magnitude across this temperature range due to band gap narrowing

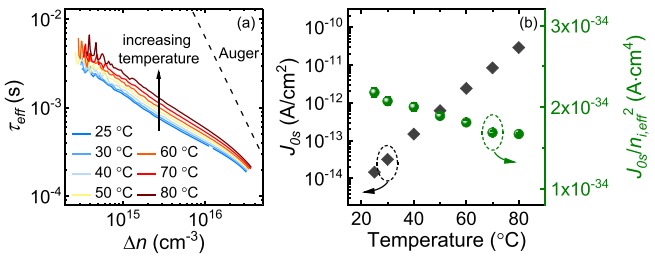

Fig. 7. (a) τ_{eff} of the symmetrical test structure as a function of Δn in the range of temperature from 25 to 80 °C and (b) J_{0s} extracted from the τ_{eff} data using Quokka and $J_{0s}/n_{i,eff}^2$ ratios as a function of temperature. The error bars in (b) were determined from R-squared values of J_{0s} fits using Quokka.

[41] and as J_{0s} is proportional to $n_{i,eff}^2$ [32], the significant increase of J_{0s} is mainly due $n_{i,eff}$. The $J_{0s}/n_{i,eff}^2$ ratios as a function of temperature are also presented in Fig. 7(b). If the temperature dependence of J_{0s} is solely determined by $n_{i,eff}$, these ratios should be temperature-independent. However, as shown in Fig. 7(b), this is not the case. A slight reduction of $J_{0s}/n_{i,eff}^2$ (green points) at elevated temperatures can be observed. This indicates a small improvement of the surface passivation with increasing temperature. However, it seems that this improvement does not have a strong impact on TC_{Voc}. The increase of $n_{i,eff}$ at elevated temperatures is still dominating the trend of V_{oc} with temperature, and hence TC_{Voc}.

4. Conclusion

The temperature dependence of poly-Si passivating contacts and their cell performance was examined and their TCs were quantified. We observed a small improvement of the surface passivation of poly-Si passivating contacts with increasing temperature. However, it seems that this improvement does not have a strong impact on TC_{Voc}. The temperature dependence of V_{oc} is still dominated by band gap narrowing at elevated temperatures. Furthermore, the absolute value of TC_{Voc} increases with decreasing illumination intensity, indicating that the investigated solar cell is more sensitive to temperature variation at lower illumination intensities. We also found that TC_{FF} of the reported TOPCon cells is superior to those of other cell structures reported in the literature and linked this to an improvement of R_s. Part of this improvement can be attributed to the decrease of ρ_c of poly-Si passivating contacts with increasing temperature. It counterbalances some of the *FF* losses, and hence, improves TC_{FF}. The determined TC_η of the investigated TOPCon solar cells is comparable to TC_η of SHJ cells and better than those of cell structures without passivating contacts, highlighting the advantage of using this advanced structure in the field.

CRediT authorship contribution statement

Anh Huy Tuan Le: Methodology, Investigation, Formal analysis, Validation, Writing – original draft. **Rabin Basnet:** Conceptualization, Investigation, Writing – review & editing. **Di Yan:** Investigation, Writing – review & editing. **Wenhao Chen:** Investigation. **Naomi Nandakumar:** Investigation, Writing – review & editing. **Shubham Duttagupta:** Investigation, Writing – review & editing. **Johannes P. Seif:** Supervision, Writing – review & editing. **Ziv Hameiri:** Supervision, Funding acquisition, Writing – review & editing.

Declaration of competing interest

The authors declare that they have no known competing financial interests or personal relationships that could have appeared to influence the work reported in this paper.

Acknowledgement

The authors thank Dr. Nino Borojevic for his help with the *I–V* measurement setup. The authors also thank Dr. Ron Sinton and his team in Sinton Instruments for building the custom-designed Suns-V_{oc} system used in this study. This work was supported by the Australian Government through Australian Renewable Energy Agency [ARENA; project 2017/RND001]. The views expressed herein are not necessarily the views of the Australian Government, and the Australian Government does not accept responsibility for any information or advice contained herein.

Appendix A. Supplementary data

Supplementary data to this article can be found online at https://doi.org/10.1016/j.solmat.2021.111020.

References

[1] IEC, Photovoltaic Devices - Part 1-10, IEC 60904, 2009.
[2] M. Kasu, J. Abdu, S. Hara, S. Choi, Y. Chiba, A. Masuda, Temperature dependence measurements and performance analyses of high-efficiency interdigitated back-contact, passivated emitter and rear cell, and silicon heterojunction photovoltaic modules, Jpn. J. Appl. Phys. 57 (2018), 08RG18.
[3] J. Haschke, J.P. Seif, Y. Riesen, A. Tomasi, J. Cattin, L. Tous, P. Choulat, M. Aleman, E. Cornagliotti, A. Uruena, R. Russell, F. Duerinckx, J. Champliaud, J. Levrat, A.A. Abdallah, B. Aissa, N. Tabet, N. Wyrsch, M. Despeisse, J. Szlufcik, S. De Wolf, C. Ballif, The impact of silicon solar cell architecture and cell interconnection on energy yield in hot & sunny climates, Energy Environ. Sci. 10 (2017) 1196–1206.
[4] S. Kurtz, K. Whitfield, G. TamizhMani, M. Koehl, D. Miller, J. Joyce, J. Wohlgemuth, N. Bosco, M. Kempe, T. Zgonena, Evaluation of high-temperature exposure of photovoltaic modules, Prog. Photovoltaics Res. Appl. 19 (2011) 954–965.
[5] M.A. Green, General temperature dependence of solar cell performance and implications for device modelling, Prog. Photovoltaics Res. Appl. 11 (2003) 333–340.
[6] F. Feldmann, M. Simon, M. Bivour, C. Reichel, M. Hermle, S.W. Glunz, Carrier-selective contacts for Si solar cells, Appl. Phys. Lett. 104 (2014) 181105.
[7] M. Tanaka, M. Taguchi, T. Matsuyama, T. Sawada, S. Tsuda, S. Nakano, H. Hanafusa, Y. Kuwano, Development of new a-Si/c-Si heterojunction solar cells: ACJ-HIT (artificially constructed junction-heterojunction with intrinsic thin-layer), Jpn. J. Appl. Phys. 31 (1992) 3518–3522.
[8] X.B. Yang, P.T. Zheng, Q.Y. Bi, K. Weber, Silicon heterojunction solar cells with electron selective TiO_x contact, Sol. Energy Mater. Sol. Cells 150 (2016) 32–38.
[9] J. Bullock, P.T. Zheng, Q. Jeangros, M. Tosun, M. Hettick, C.M. Sutter-Fella, Y. Wan, T. Allen, D. Yan, D. Macdonald, S. De Wolf, A. Hessler-Wyser, A. Cuevas, A. Javey, Lithium fluoride based electron contacts for high efficiency n-type crystalline silicon solar cells, Adv Energy Mater 6 (2016) 1600241.
[10] J. Bullock, C. Samundsett, A. Cuevas, D. Yan, Y. Wan, T. Allen, Proof-of-concept p-type silicon solar cells with molybdenum oxide local rear contacts, IEEE J Photovolt 5 (2015) 1591–1594.
[11] J. Bullock, M. Hettick, J. Geissbühler, A.J. Ong, T. Allen, C.M. Sutter-Fella, T. Chen, H. Ota, E.W. Schaler, S. De Wolf, Efficient silicon solar cells with dopant-free asymmetric heterocontacts, Nat Energy 1 (2016) 1–7.
[12] A. Cuevas, Y.M. Wan, D. Yan, C. Samundsett, T. Allen, X.Y. Zhang, J. Cui, J. Bullock, Carrier population control and surface passivation in solar cells, Sol. Energy Mater. Sol. Cells 184 (2018) 38–47.
[13] J. Melskens, B.W.H. van de Loo, B. Macco, L.E. Black, S. Smit, W.M.M. Kessels, Passivating contacts for crystalline silicon solar cells: from concepts and materials to prospects, IEEE J Photovolt 8 (2018) 373–388.
[14] J. Schmidt, R. Peibst, R. Brendel, Surface passivation of crystalline silicon solar cells: present and future, Sol. Energy Mater. Sol. Cells 187 (2018) 39–54.
[15] T.G. Allen, J. Bullock, X.B. Yang, A. Javey, S. De Wolf, Passivating contacts for crystalline silicon solar cells, Nat Energy 4 (2019) 914–928.
[16] F. Haase, C. Hollemann, S. Schafer, A. Merkle, M. Rienacker, J. Krugener, R. Brendel, R. Peibst, Laser contact openings for local poly-Si-metal contacts enabling 26.1%-efficient POLO-IBC solar cells, Sol. Energy Mater. Sol. Cells 186 (2018) 184–193.
[17] J. Bullock, Y.M. Wan, M. Hettick, Z.R. Xu, S.P. Phang, D. Yan, H.C. Wang, W.B. Ji, C. Samundsett, Z. Hameiri, D. Macdonald, A. Cuevas, A. Javey, Dopant-free partial rear contacts enabling 23% silicon solar cells, Adv Energy Mater 9 (2019) 1803367.
[18] N. Nandakumar, J. Rodriguez, T. Kluge, T. Grosse, L. Fondop, P. Padhamnath, N. Balaji, M. Konig, S. Duttagupta, Approaching 23% with large-area monoPoly cells using screen-printed and fired rear passivating contacts fabricated by inline PECVD, Prog. Photovoltaics Res. Appl. 27 (2019) 107–112.
[19] W.L. Wu, W.J. Lin, S.H. Zhong, B. Paviet-Salomon, M. Despeisse, Q. Jeangros, Z. C. Liang, M. Boccard, H. Shen, C. Ballif, Dopant-free back-contacted silicon solar cells with an efficiency of 22.1%, Phys Status Solidi-R 14 (2020) 1900688.

[20] K. Yoshikawa, H. Kawasaki, W. Yoshida, T. Irie, K. Konishi, K. Nakano, T. Uto, D. Adachi, M. Kanematsu, H. Uzu, K. Yamamoto, Silicon heterojunction solar cell with interdigitated back contacts for a photoconversion efficiency over 26%, Nat Energy 2 (2017) 17032.

[21] D. Adachi, J.L. Hernandez, K. Yamamoto, Impact of carrier recombination on fill factor for large area heterojunction crystalline silicon solar cell with 25.1% efficiency, Appl. Phys. Lett. 107 (2015) 233506.

[22] M. Taguchi, A. Yano, S. Tohoda, K. Matsuyama, Y. Nakamura, T. Nishiwaki, K. Fujita, E. Maruyama, 24.7% record efficiency HIT solar cell on thin silicon wafer, IEEE J Photovolt 4 (2014) 96–99.

[23] R. Basnet, S.P. Phang, C. Samundsett, D. Yan, W.S. Liang, C. Sun, S. Armand, R. Einhaus, J. Degoulange, D. Macdonald, 22.6% efficient solar cells with polysilicon passivating contacts on n-type solar-grade wafers, Sol Rrl 3 (2019) 1900297.

[24] A. Richter, J. Benick, F. Feldmann, A. Fell, M. Hermle, S.W. Glunz, n-type si solar cells with passivating electron contact: identifying sources for efficiency limitations by wafer thickness and resistivity variation, Sol. Energy Mater. Sol. Cells 173 (2017) 96–105.

[25] F. Feldmann, M. Bivour, C. Reichel, M. Hermle, S.W. Glunz, Passivated rear contacts for high-efficiency n-type Si solar cells providing high interface passivation quality and excellent transport characteristics, Sol. Energy Mater. Sol. Cells 120 (2014) 270–274.

[26] J. Krügener, Y. Larionova, D. Tetzlaff, B. Wolpensinger, S. Reiter, M. Turcu, R. Peibst, J.-D. Kähler, T. Wietler, Dopant diffusion from p^+-poly-Si into c-Si during thermal annealing, 43rd IEEE Photovoltaic Specialists Conference, 2016, pp. 2451–2454.

[27] N. Nandakumar, J. Rodriguez, T. Kluge, T. Grosse, D. Landgraf, N. Balaji, M. Esber, P. Padhamnath, S. Duttagupta, 6% monoPoly™ cells with in-situ interfacial oxide and poly-Si layers deposited by inline PECVD, 7th World Conference on Photovoltaic Energy Conversion, 2018, pp. 2048–2051.

[28] S. Duttagupta, N. Nandakumar, R. Stangl, A.G. Aberle, Initial Results of monoPoly™ Silicon Solar Cells at SERIS, 7th World Conference on Photovoltaic Energy Conversion, 2018, pp. 1991–1994.

[29] W. Kern, The evolution of silicon-wafer cleaning technology, J. Electrochem. Soc. 137 (1990) 1887–1892.

[30] R. Basnet, F.E. Rougieux, C. Sun, S.P. Phang, C. Samundsett, R. Einhaus, J. Degoulange, D. Macdonald, Methods to improve bulk lifetime in n-type Czochralski-grown upgraded metallurgical-grade silicon wafers, IEEE J Photovolt 8 (2018) 990–996.

[31] D. Yan, S.P. Phang, Y.M. Wan, C. Samundsett, D. Macdonald, A. Cuevas, High efficiency n-type silicon solar cells with passivating contacts based on PECVD silicon films doped by phosphorus diffusion, Sol. Energy Mater. Sol. Cells 193 (2019) 80–84.

[32] D. Kane, R. Swanson, Measurement of the emitter saturation current by a contactless photoconductivity decay method, 18th IEEE Photovoltaic Specialists Conference, 1985, pp. 578–583.

[33] T.C. Kho, K. Fong, K. McIntosh, E. Franklin, N. Grant, M. Stocks, S.P. Phang, Y. Wan, E.-C. Wang, K. Vora, Exceptional silicon surface passivation by an ONO dielectric stack 189 (2019) 245–253.

[34] D. Yan, A. Cuevas, J. Bullock, Y. Wan, C. Samundsett, Phosphorus-diffused polysilicon contacts for solar cells 142 (2015) 75–82.

[35] R.H. Cox, H. Strack, Ohmic contacts for GaAs devices, Solid State Electron. 10 (1967) 1213–1218.

[36] J.P. Seif, T.G. Allen, Z. Hameiri, Temperature-dependent Suns-V_{oc} and Suns-PL Method for Advanced Characterization of Solar Cells, Asia-Pacific Solar Research Conference, 2019.

[37] M. Wolf, H. Rauschenbach, Series resistance effects on solar cell measurements, Adv. Energy Convers. 3 (1963) 455–479.

[38] C. Vargas, Y. Zhu, G. Coletti, C. Chan, D. Payne, M. Jensen, Z. Hameiri, Recombination parameters of lifetime-limiting carrier-induced defects in multicrystalline silicon for solar cells, Appl. Phys. Lett. 110 (2017), 092106.

[39] A. Fell, A free and fast three-dimensional/two-dimensional solar cell simulator featuring conductive boundary and quasi-neutrality approximations, IEEE Trans. Electron. Dev. 60 (2013) 733–738.

[40] R. Dumbrell, M.K. Juhl, T. Trupke, Z. Hameiri, Extracting metal contact recombination parameters from effective lifetime data 8, 2018, pp. 1413–1420.

[41] A. Schenk, Finite-temperature full random-phase approximation model of band gap narrowing for silicon device simulation, J. Appl. Phys. 84 (1998) 3684–3695.

[42] R. Couderc, M. Amara, M. Lemiti, Reassessment of the intrinsic carrier density temperature dependence in crystalline silicon, J. Appl. Phys. 115 (2014), 093705.

[43] A. Richter, S.W. Glunz, F. Werner, J. Schmidt, A. Cuevas, Improved quantitative description of Auger recombination in crystalline silicon, Phys. Rev. B 86 (2012) 165202.

[44] D.B.M. Klaassen, A unified mobility model for device simulation—I. Model-equations and concentration-dependence, Solid State Electron. 35 (1992) 953–959.

[45] R. Pässler, Semi-empirical descriptions of temperature dependences of band gaps in semiconductors, Phys. Status Solidi 236 (2003) 710–728.

[46] F. Feldmann, G. Nogay, P. Loper, D.L. Young, B.G. Lee, P. Stradins, M. Hermle, S. W. Glunz, Charge carrier transport mechanisms of passivating contacts studied by temperature-dependent J-V measurements, Sol. Energy Mater. Sol. Cells 178 (2018) 15–19.

[47] M.A. Green, K. Emery, A.W. Blakers, Silicon solar-cells with reduced temperature sensitivity, Electron. Lett. 18 (1982) 97–98.

[48] M.A. Green, Solar Cells: Operating Principles, Technology, and System Applications, Prentice-Hall, Englewood Cliffs, NJ, USA, 1982.

[49] O. Dupré, R. Vaillon, M.A. Green, Thermal Behavior of Photovoltaic Devices, Springer, Switzerland, 2017.

[50] O. Dupré, R. Vaillon, M.A. Green, Experimental assessment of temperature coefficient theories for silicon solar cells, IEEE J Photovolt 6 (2016) 56–60.

[51] R. Eberle, A. Fell, S. Mägdefessel, F. Schindler, M.C. Schubert, Prediction of local temperature-dependent performance of silicon solar cells, Prog. Photovoltaics Res. Appl. 27 (2019) 999–1006.

[52] S.T. Kristensen, S. Nie, C. Berthod, R. Strandberg, J.O. Odden, Z. Hameiri, How gettering affects the temperature sensitivity of the implied open circuit voltage of multicrystalline silicon wafers, in: 46th IEEE Photovoltaic Specialists Conference, 2019, 0061–0067.

[53] S. Nie, S.T. Kristensen, A. Gu, R.L. Chin, T. Trupke, Z. Hameiri, Photoluminescence-based spatially resolved temperature coefficient maps of silicon wafers and solar cells, IEEE J Photovolt 10 (2020) 585–594.

[54] C.Q. Xiao, D.R. Yang, X.G. Yu, X. Gu, D.L. Que, Influence of the compensation level on the performance of p-type crystalline silicon solar cells: theoretical calculations and experimental study, Sol. Energy Mater. Sol. Cells 107 (2012) 263–271.

[55] A. Luque, S. Hegedus, Handbook of Photovoltaic Science and Engineering, John Wiley & Sons, 2011.

[56] C.Q. Xiao, X.G. Yu, D.R. Yang, D.L. Que, Impact of solar irradiance intensity and temperature on the performance of compensated crystalline silicon solar cells, Sol. Energy Mater. Sol. Cells 128 (2014) 427–434.

[57] S. Ponce-Alcantara, J.P. Connolly, G. Sanchez, J.M. Miguez, V. Hoffmann, R. Ordas, A statistical analysis of the temperature coefficients of industrial silicon solar cells, 4th International Conference on Crystalline Silicon Photovoltaics 55 (2014) 578–588.

[58] H. Haug, C. Berthod, A. Skomedal, J.O. Odden, E.S. Marstein, R. Sondena, Simulated and measured temperature coefficients in compensated silicon wafers and solar cells, Sol. Energy Mater. Sol. Cells 200 (2019) 109921.

[59] Z.C. Holman, M. Filipič, B. Lipovšek, S. De Wolf, F. Smole, M. Topič, C. Ballif, Parasitic absorption in the rear reflector of a silicon solar cell: simulation and measurement of the sub-bandgap reflectance for common dielectric/metal reflectors, Sol. Energy Mater. Sol. Cells 120 (2014) 426–430.

[60] Z.C. Holman, S. De Wolf, C. Ballif, Improving metal reflectors by suppressing surface plasmon polaritons: a priori calculation of the internal reflectance of a solar cell, Light Sci. Appl. 2 (2013) e106.

[61] S. Glunz, J. Nekarda, H. Mäckel, A. Cuevas, Analyzing back contacts of silicon solar cells by Suns-V_{oc}-measurements at high illumination densities, 22nd European Photovoltaic Solar Energy Conference 3 (2007) 849–853.

[62] R. Dumbrell, M.K. Juhl, T. Trupke, Z. Hameiri, Comparison of terminal and implied open-circuit voltage measurements, IEEE J Photovolt 7 (2017) 1376–1383.

[63] J. Bullock, C. Samundsett, A. Cuevas, F. Yan, Y.M. Wan, T. Allen, Proof-of-concept p-type silicon solar cells with molybdenum oxide local rear contacts, IEEE J Photovolt 5 (2015) 1591–1594.

[64] N. Folchert, M. Rienacker, A.A. Yeo, B. Min, R. Peibst, R. Brendel, Temperature-dependent contact resistance of carrier selective poly-Si on oxide junctions, Sol. Energy Mater. Sol. Cells 185 (2018) 425–430.

[65] P. Singh, S.N. Singh, M. Lal, M. Husain, Temperature dependence of I-V characteristics and performance parameters of silicon solar cell, Sol. Energy Mater. Sol. Cells 92 (2008) 1611–1616.

[66] E. Cuce, P.M. Cuce, T. Bali, An experimental analysis of illumination intensity and temperature dependency of photovoltaic cell parameters, Appl. Energy 111 (2013) 374–382.

[67] D.L. Meier, E.A. Good, R.A. Garcia, B.L. Bingham, S. Yamanaka, V. Chandrasekaran, C. Bucher, Determining components of series resistance from measurements on a finished cell, 4th World Conference on Photovoltaic Energy Conversion, 2006, pp. 1315–1318.